A Reconfigurable Multi-Band Notched Semi-Circle Engraved UWB Antenna for Wireless Applications

Subhash Shrimal[1$*], Renu Agrawal [2$], Indra Bhooshan Sharma[3$], Joohi Garg[4$], and M. M. Sharma[5$]
[$]Department of ECE, Malaviya National Institute of Technology, Jaipur, India-302017
*Corresponding Author Mobile Number - +91-9413333436
[1]2019rec9534@mnit.ac.in, [2]2019rec9553@mnit.ac.in, [3]2019rec9064@mnit.ac.in, [4]2019rec9530@mnit.ac.in, [5]mms.ece@mnit.ac.in
1. *Present address: Department of Electronics and Communication Engineering, Malaviya National Institute of Technology, JLN Marg Jaipur, India-302017*

Abstract: This work presents a small reconfigurable UWB (Ultra-Wide-Band) antenna with quad-band notches that may be used for multi-notching bands and anti-interference. It consists of a semi-circle engraved stepped-cut monopole antenna with two bevels. The slotted ground is also provided with two bevels to get enhanced bandwidth, from 3.1 to 11.67 GHz (116%). The two bevels also aid in achieving impedance matching, particularly over 9.9 GHz. To get notch characteristics covering the 5G band in 3.40-3.70 GHz (n78) and 4.84-5.70 GHz (n46), the patch is provided with L-shaped and Ladder-shaped stubs of quarter wavelength. A band-notch function is obtained at 3.88-4.32 GHz (n77, C-band), 7.10-7.61 GHz (X-band satellite downlink), and 8.04-8.68 GHz (ITU-8 GHz) by incorporating a half wavelength C-shaped slot, an I-shaped stub on the patch, and two RSRRs close to microstrip feed-line. The suggested antenna has eight PIN diodes that regulate several operating modes, allowing it to accomplish single/double/triple/quadruple band-notch characteristics. The size of the patch is $0.25\lambda \times 0.37\lambda$ mm^2 and printed on Rogers RT/duroid-5880 substrate. The simulated, measured, and equivalent circuit results match well with each other. It offers a stable gain and acceptable radiation pattern throughout the UWB band except for notch bands.

Keywords: Reconfigurable, UWB antenna, band notch, PIN diode, Rectangular Split Ring Resonators (RSRRs), 5G Sub-6 GHz bands.

1. Introduction

In 2002, the Federal Communications Commission (FCC) declared 3.1–10.6 GHz, the frequency range used by UWB technology, to be an unlicensed spectrum for radio transmission, with a radiated power of maximum value 41.3 dBm/MHz and an information throughput of 110-200 Mbps across a 10-meter distance [1,2]. The UWB antennas have recently become the most often utilized antennas due to various appealing properties i.e., low cost, lightweight, and low profile. It is utilized in various applications, including short-range high data rate wideband communication, satellite, cognitive radio, radar sensing, aircraft, and

body area networking [3]. A very low transmission power level is permitted by FCC for UWB systems, due to narrowband communications i.e., Wi-Max, C-band, WLAN, and 5G Sub 6 GHz band applications [4]. A band-reject filter is used to mitigate the narrowband interference in UWB systems. However, it will raise the system's size, cost, and complexity. So, band-notch technique is preferable to prevent interference in a UWB antenna [5-7].

UWB antennas employing single [8-10], dual [11-13], or triple [14-15] band rejection capabilities have been described to avoid possible interference. Recently, there have been descriptions of UWB antennas with four or more notch bands [16-17]. When an antenna is excited for radiation, all signals excluding notched bands will radiate. However, selective control of radiation in notched bands is not possible. To achieve this selective control or efficient use of the UWB spectrum, an antenna with one or more notched band characteristics must be designed to allow controlled operation using electrical switching that alters the current distribution in the OFF-ON mode. A variety of switch types as RF-MEMS *(Micro-Electro-Mechanical System)*, optical switches, PIN diodes, varactors, FETs (Field-effect transistors), and so on are utilized for achieving reconfigurability [18-32]. According to [21], an improved radiating stub with two protruding arrow-shaped strips can have a PIN diode across it to create a reconfigurable single band-notched feature for WLAN (5–6 GHz). In [22], a single reconfigurable notch band (3.5–4.95 GHz), including C-band and Wi-MAX, is accomplished by placing a switch across the poles of the G-shaped ring radiator. Nevertheless, in the UWB frequency range, a single-notch band with reconfigurability is not enough to eliminate the interference. An elliptical SRR with two PIN diodes and a PIN diode positioned in two strips having a T-shape makes up the reconfigurable antenna at 3.3–3.85 GHz and 5.1–6.0 GHz described in [23]. A circular ring radiator with a T-shaped stub and a semi-circular parasitic strip coupled by PIN diodes in [24] offers reconfigurable dual-band notch features. In order to notch the interfering frequencies at 3.30–3.60 GHz, 5.725–5.825 GHz, and 3.70–4.20 GHz, a reconfigurable antenna contains three notch bands with two stubs and a slot is provided between the radiator and feed line as suggested in [25]. As stated in [26], a rectangular patch that may be reconfigured using three PIN diodes has two arms of C-shaped along the patch sides and a slot of H-shape on its surface to notch triple bands. A feed-line using a U-shaped slot, two SRRs near to feed-line, a ring resonator, and a patch with few T-like resonators are described in [27]. This structure employs five different switches to enable reconfigurable design with quadruple notches at 3.5, 5.3, 5.8, and 7.4 GHz. The proposed reconfigurable multi-band-notched antenna is designed to function across a wide range of frequencies, including UWB, as well as single, dual, triple, and quadruple-

band notches. The compact design of the antenna allows it to effectively reject common interfering 5G Sub-6 GHz bands such as n78 (3.40-3.70 GHz), n46 (4.84-5.70 GHz), and n77 (3.88-4.32 GHz), employing distinct switching conditions. Additionally, it provides notches for interfering bands like ITU-8 GHz (8.04-8.68 GHz) and X-band downlink (7.10-7.61 GHz). These frequency bands are crucial for widespread deployment in both urban and rural settings due to their capacity and coverage balance. The antenna's performance has been validated through measurements, simulations, and equivalent circuit analysis, indicating its effectiveness. Apart from the notch bands, the antenna maintains consistent gain and radiation efficiency, with peak values of 4.26 dBi and 86%, respectively, across the 3.15-11.88 GHz range. This suggests that a variety of UWB applications, resilient to interference from neighboring RF systems, can be supported by the antenna. An equivalent circuit model analysis, which depicts the operation of notched bands according to circuit theory, is investigated to analyze the aforementioned antennas [34-36].

The suggested reconfigurable antenna has two bevels on the partially slotted ground and two bevels in the bottom edge of the stepped cut patch, showing increased impedance bandwidth from 3.1-11.67 GHz (116%). The structure consists of two RSRRs across the microstrip feed line, three stubs, and a slot in the patch, all of which are controlled by PIN diodes. The antenna has numerous operation modes with notch states in single, dual, triple, and quadruple bands for different interference scenarios. These modes are realized by switching PIN diodes, managed by appropriate biasing. Section 2 of the paper discussed the analysis and design components of the suggested antenna. The parametric analysis of notch bands is examined in Section 3. PIN diode-based control mechanism is covered in Section 4. The simulated results are discussed and verified with measured results in Section 5.

2. Antenna design and analysis

2.1. Design and Geometry of the Antenna

The suggested antenna is fabricated with the design shown in Fig. 1(a), with an 18.5 × 29.5 mm^2 Rogers RT/duroid5880 substrate, 2.2 relative permittivity, 0.762 mm thickness, and a 0.0009 loss tangent. It is supplied via a 50 Ω feed line with optimal dimensions of W_f *X* L_f. A stepwise analysis is conducted to understand how the antenna with notched bands evolved, as Fig. 2 illustrates. The fundamental antenna structure is depicted in Fig.2(a), which comprises a rectangular patch with an engraved semicircle and a partial ground that minimizes the area of the patch. To improve the S_{11} bandwidth, two bevels are inserted in the ground and radiator as depicted in Fig.2(b), which is controllable by varying the bevels' dimensions. This

increases the S_{11} bandwidth beyond 9.30 GHz and covers the span of 3.1-11.67 GHz (116%), which is useful for a variety of wireless applications. Currently, a lot of wireless services operating in the above frequency spectrum interfere with one another and must be eliminated by modifying the antenna. As shown in Figs. 2(c) to 2(g), the antenna can be modified by either etching slots or inserting a stub.

The antenna, as depicted in Figs. 1(a) and 1(b), has a radiator-like front view and a ground-like rear view, respectively. To achieve notch characteristics in 3.30–3.68 GHz (f_{Notch}=3.5 GHz) and 5.15–5.82 GHz (f_{Notch}=5.5 GHz) bands, quarter-wavelength L- and ladder-shaped stubs are placed in the radiating patch's rhombic-shaped slot. A pair of RSRRs near the microstrip feedline, an I-shaped stub, and a C-shaped slot of half wavelengths are used to achieve notch bands with high band rejection (VSWR > 16) at 8.14–8.83 GHz (f_{Notch}=8.5 GHz), 7.25–7.75 GHz (f_{Notch}=7.5 GHz), and 3.80 – 4.40 GHz (f_{Notch}=4.1 GHz) respectively.

Several factors are taken into account while optimizing the suggested antenna, including radiation patterns, band rejection level, antenna bandwidth, and bandwidth of the notch bands. The CST simulator tool optimizes the suggested antenna's dimensions, as indicated in Table 1. The distinct notched bands are controlled by PIN diodes (*Skyworks SMP1320-079LF*), which yield reconfigurability. Eight PIN switches are incorporated to get the necessary reconfigurable characteristics of the suggested design, as shown in Fig. 1(c).

2.2 Design of Notch Elements

A notch element is made to be roughly half of its wavelength $(\lambda_g/2)$ in length at f_{Notch} (center frequency of notch band). It will resonate at f_{Notch}, forcing the current to flow in the opposite direction on both sides of the slot, making it impossible to emit or receive EM waves in the notch band. The following formulas can be used to empirically estimate the overall length of the suggested notch-band (band-stop) elements [34].

$$L_{NotchBand} \approx \frac{\lambda_g}{2} = \frac{\lambda_0}{2\sqrt{\varepsilon_{reff}}} \quad (1)$$

$$L_{NotchBand} = \frac{c}{2 \times f_{Notch}\sqrt{\varepsilon_{reff}}} \quad (2)$$

$$\varepsilon_{reff} \approx \frac{\varepsilon_r + 1}{2} \quad (3)$$

where c, λ_0, λ_g, and ε_{reff} represent free space EM wave speed, free space wavelength, guided wavelength, and dielectric constant of the substrate, respectively. The band-stop element's fractional bandwidth (FBW) and notch frequency (f_{Notch}) may be expressed as follows, with input impedance decreasing to $1/\sqrt{2}$ of the maximum level.

$$f_{Notch} = \frac{1}{2\pi\sqrt{L_{eq}C_{eq}}} \quad (4)$$

$$FBW = \frac{f_2 - f_1}{f_{Notch}} = \frac{1}{Q} \quad (5)$$

where Q, L_{eq}, and C_{eq} stand for the recommended equivalent circuit's quality factor, capacitance, and inductance, respectively.

To obtain the suggested antenna's structure the seven design stages are described in Fig. 2. Initially, Fig. 2(a) shows the enhanced UWB antenna-2 and the partial UWB antenna-1. The 5G Sub-6 GHz spectrum from 5.15 to 5.82 GHz is eliminated as a result of an L-shaped open stub of a quarter wavelength, as depicted in Fig. 2(c). $L_{n46} = L_1+L_2 = 12.80$ mm is the length of the L-shaped stub. A ladder-shaped band rejection element of quarter wavelength is attached to the L-shaped stub as depicted in Fig. 2(d) to provide a reasonably acute and precise notched n78-5G band from 3.30–3.68 GHz. $L_{n78} = 31.10$ mm is the n78 band notch element length. Fig. 2(e) shows that a C-shaped slot is inserted to eliminate the n77-5G band (3.80–4.40 GHz). It has a length of $L_{n77} = 2(L_{11}+L_{12}) = 30.8$ mm. As depicted in Fig. 2(g), two RSRR band stop filters are positioned across the feed line to generate a relatively wide stopband for the frequency range of 8.14 to 8.83 GHz (ITU-8 GHz). Similarly, an I-shaped stub is used as indicated in Fig. 2(f) to suppress the band 7.25 to 7.75 GHz. The I-shaped and RSRRs band-stop filter has the following lengths: $L_{ITU} = 2*(L_{16}+L_{17})-a = 15.6$ mm and $L_X = 2(L13-2g_2) + 2(L_{14}-3g_2) + 2L_{15} = 18.20$ mm, respectively.

The comparison of the reflection coefficients [S_{11}] for different stages of the suggested antenna is illustrated in Fig. 3. Antenna-1 covers a partial UWB spectrum of 3.27-9.30 GHz, whereas antenna 2 covers the UWB band with an improved bandwidth of 3.1-11.67 GHz as shown in Fig. 3(a). Single, dual, triple, and quadruple notch bands are displayed in subsequent antenna stages, accordingly as depicted in Fig. 3(b). Antenna-2 displays an excellent impedance match across the operating band with VSWR < 2, whereas other antenna designs show significant notch characteristics with VSWR > 16 as depicted in Fig. 4.

3. Parametric analysis of notch bands

The antenna performance analysis that uses notch structure parameters is shown in Fig. 5. A full-wave EM solver is used to optimize and examine the suggested antenna's parameters. It confirms equation (2) as any variation in slot or stub length while maintaining other dimensions fix, shifts the center frequency inversely. The current path will also be extended in conjunction with the increase in slot length. As a result, as Table 2 summarises, it is possible to control each notch band independently by modifying the slot's or stub's length, breadth, and placement without affecting the other notch bands.

4. Reconfigurable characteristics

The bias circuit modifies the antenna's current distribution and enables reconfigurability by controlling the ON-OFF positions of diodes at various slots [19]. The suggested bias circuit as shown in Fig. 1(d) connects terminals A1 and A2 over an L-shaped stub, terminals B1 and B2 across a Ladder-shaped stub, terminals C1-C2 and G1-G2 via a C-shaped slot, terminals D1-D2 and H1-H2 across an I-shaped stub, and terminals E1-E2 and F1-F2 across an RSRR. The direct current (DC) power supply is isolated by the capacitor *(C=22 pF with part no. VJ0603A220JXAAC)*, which also keeps DC power from influencing the suggested antenna's radiation. The RF signal is suppressed using the inductance *(L=68 nH with part no. LQG15WZ68NH02D)* in order to avoid the DC power supply becoming unstable due to input signal. To safeguard the device and restrict the amount of current passing through the diode, a resistor *(R=220 Ohm with part no. CRCW0201220RFNED)* is utilized. The reconfigurability of the antenna is accomplished by managing diode states by connecting various configurations of the eight +ve polarity to the -ve polarity of the DC supply. By varying the PIN diodes' state, the quadruple-notch bands may be separately controlled to conduct the antenna's operation modes under different interference scenarios, as described in Table 3.

5. Validation and discussion of simulated with experimental results

The suggested novel reconfigurable antenna is verified by fabricating and measuring a prototype, which is depicted in Fig. 6(a, b) for the top and bottom layers. A Network Analyzer Keysight M9808A is used to measure reflection coefficients, and an anechoic chamber as shown in Fig. 6(d) is used to measure all radiation characteristics, including gain, efficiency, and radiation patterns.

5.1 Reflection Coefficient Measurement

Fig. 7 illustrates the Reflection Coefficient simulation and measuring results for the different switching modes of the suggested antenna. There is a satisfactory agreement between these results. The measurement environment, SMA connector losses, PIN diode model, and fabrication process are all responsible for the little variations in measured results.

Fig. 7(e) indicates that the ON states of PIN diodes D3, D4, D7, and D8 (Mode-11) cover the whole UWB band (3.15-11.88 GHz), which causes the current concentration across the relevant notch element to disappear. For all diodes in the ON state (Mode-10), dual notch bands are created to prevent interference due to (3.55-3.90 GHz, 5G-n78 band) and (7.93-8.95 GHz, ITU-8 GHz) bands. Two PIN diodes (D1 and D2), along with the ON states of PIN diodes D3, D4, D7, and D8, are what control how the suggested reconfigurable antenna operates in notch bands 4.84-5.70 GHz and 3.34-3.75 GHz, as indicated in Fig. 7(a). It displays a notch in the 5G-n46 band when D1 is ON (Mode-1), and a notch in the 5G-n78 band when D1, and D2 are in the ON state (Mode-2). It is also noted that when PIN diodes D3 (Mode-3), D4 (Mode-4), and D5 (Mode-5) are in the ON condition, the antenna offers a single notch band in (3.93-4.51 GHz, C band), (7.14-7.59 GHz, X-band satcom), and (7.85-8.70 GHz, ITU-8 GHz band) respectively as illustrated in Fig. 7(b). Also, it provides a dual notch when PIN diodes D1, D2, and D3 are turned on in Mode-6, as depicted in Fig. 7(c). For 3.30–4.20 GHz and 7.10–7.80 GHz, the antenna further implements a dual notch for the ON state of PIN diodes D3 and D4 (Mode-7). As depicted in Fig. 7(d), it may block triple interference signals at 3.22-3.55 GHz, 3.75-4.28 GHz, and 7.30-7.86 GHz in Mode-8. Similarly, to generate the quadruple notch bands (Mode-9) at 3.40-3.70 GHz, 3.88-4.32 GHz, 7.10-7.61 GHz, and 8.04-8.68 GHz bands, PIN diodes D5 and D6 are turned on in conjunction with Mode-8.

5.2 Analysis of surface current distribution

One may evaluate the effect of the notching structure by examining the antenna's surface current distribution. It explains how slots and stubs are used to introduce notch bands. Fig. 8 shows the current distributions at five distinct notched frequencies (3.5, 5.5, 4.1, 7.5, and 8.5 GHz) to help comprehend the working concept underlying this quadruple band-notched performance. The antenna's band-notching characteristic is caused by significant impedance mismatches at the resonant frequencies, which are caused by the currents being mostly centered at these frequencies surrounding the slot resonators.

5.3 Radiation Pattern

In two main planes (yz and xz), the radiation patterns of simulated and measured co and cross-polarizations at different pass-band frequencies 3.7 GHz, 6.4 GHz, 9.5 GHz, and 11.0 GHz are displayed in Fig. 9. It demonstrates that in the E-plane (yz-plane), the antenna can retain its bidirectional `8' shape radiation, and in the H-plane (yz-plane), it can maintain its omnidirectional behaviour. Because the region of radiation grows with frequency, the cross-polarization increases with frequency and is less at lower frequencies. Higher-order modes are created at higher frequencies, which disturbs the phase distribution and degrades the radiation pattern of the antenna. Fig. 9 illustrates that the results obtained with cross-polarization are about 20 dB lower than those obtained with co-polarization.

5.4 Gain, Efficiency, and Group Delay

The radiation efficiency and overall gain both reach a maximum of 86% and 4.26 dBi, respectively, as indicated in Fig. 10(a). At notch band frequencies, there is a noticeable loss in gain and efficiency, confirming that the antenna does not transmit in these quadruple-notched bands. The measured radiation efficiencies are only 26%, 33%, 31%, and 34% at 3.5, 4.1, 7.5, and 8.5 GHz, respectively. The key component of time domain analysis used to quantify distortion is group delay [28]. By positioning two antennas 30 cm apart and facing each other, a uniform group delay response is obtained as depicted in Fig.10(b), except notch bands. It demonstrates that in the four intended notch bands, the variation in group delay is more than 1 ns.

A comparison of the suggested antenna and previously published work is presented in Table 4. It illustrates that the antenna has a small size with multimode reconfigurable quadruple band notch functions.

5.5 Analysis of Input impedance and equivalent circuit model

Due to the complexity and compactness of UWB antenna configurations, it is challenging to comprehend the explanation of antenna circuit theory without corresponding circuit analysis. By taking into account the simulated impedance characteristic of the suggested antenna, a recommended equivalent circuit model (ECM) is produced. The impedance characteristic of the suggested antenna, which originated from the CST simulation, is shown in Figs. 11(d, e). The analysis is then performed by creating an ECM model. The corresponding circuit without notched bands is depicted in Fig.11(a) as a sequence of linked parallel RLC circuits [34]. The complex form of the input impedance (Z_{La}) of a UWB antenna is represented as:

$$Z_{La} = \sum_{j=1}^{n} \frac{\left[j\omega R_j L_j \right]}{\left[R_j \left(1 - \omega^2 L_j C_j \right) + j\omega L_j \right]} \quad (6)$$

The antenna's input impedance graph without notches is depicted in Fig.11(d). As expected, the imaginary value of impedance is 0 Ω, while the real value is around 50 Ω, to facilitate better matching. An equivalent circuit analysis is performed for the interfering bands (5G-n78/n77/X/ITU-8 GHz band) using the input impedance shown in Fig. 11(e). A high mismatch condition must be met to eliminate interfering bands. The proposed antenna, featuring a single notch band for the n77 band of 5G sub-6 GHz at 3.5 GHz, displays a series resonance characteristic in its imaginary component curve. This occurs as the imaginary impedance transitions from negative to positive values, while the real part consistently hovers around 22 Ω. Consequently, the antenna's radiation performance diminishes at this frequency due to impedance mismatching. Similarly, the imaginary curve exhibits a series resonance characteristic at the center frequencies of 4.5 GHz and 8.5 GHz, with real impedance values close to 16 Ω and 6 Ω, respectively. Additionally, the real portion peaks at around 210 Ω at 7.50 GHz. A feature of parallel resonance is noticeable in the imaginary component curve for X-band satellite downlink communication. At this frequency, the antenna's radiation effectiveness is compromised due to the parallel resonant phenomenon opening the input terminal. Emphasis is placed on understanding input impedance throughout the study, with subsequent simulation of the relevant circuit model using CST Design Studio. Adjusting component values and configurations within the circuit simulation software allows for iterative refinement of the antenna design to meet specific performance requirements and optimize its functionality for its intended applications. As illustrated in Fig. 11(b), the suggested antenna's ECM model has two series RLCs coupled to a series RLC via a parallel RLC circuit. Moreover, it has a parallel connection to a series of resonance impedances (Z_{La}). The following formulas are used to calculate all relevant parameters [35].

$$\omega_s = \frac{1}{\sqrt{L_{sn} C_{sn}}} \quad (8)$$

$$BW_s = \frac{R_{sn}}{L_{sn}} \quad (9)$$

$$\omega_P = \frac{1}{\sqrt{L_{pn} C_{pn}}} \quad (10)$$

$$BW_p = \frac{1}{R_{pn} C_{pn}} \quad (11)$$

where the corresponding resonance frequencies for the series and parallel equivalent circuits are $\omega_s = 2\pi f_s$ & $\omega_p = 2\pi f_p$. The bandwidth for series and parallel, as determined by the simulated curve, is represented as BW_s and BW_p. Additionally, from Fig. 11(e) of the quadruple notched band antenna, R_{sn} and R_{pn} $(n = 1, 2, 3, 4...)$ are noted. The input is shorted as a result of the series components (R_{s1}, L_{s1}, C_{s1}), (R_{s2}, L_{s2}, C_{s2}), and (R_{s4}, L_{s4}, C_{s4}) resonating at 3.5, 4.5, and 8.5 GHz, respectively. In addition, an open characteristic for the input is produced by the 7.5 GHz parallel components R_{p3}, L_{p3}, and C_{p3}. As a result, the antenna is unable to radiate at the rejected bands. Additionally, a comparison is made between the simulated, measured, and ECM model's reflection coefficient curve of the suggested antenna, as illustrated in Fig. 11(f). Table 5 lists the optimized parameters of the ECM model.

5.6 Limitations of the Proposed Work

The incorporation of p-i-n diodes for achieving reconfigurability introduces parasitic characteristics that can compromise antenna performance. Specifically, these diodes, when directly linked to the radiators through biasing elements, can distort the radiation pattern and decrease RF isolation while increasing interference. In this paper, these adverse effects are reduced by using a biasing circuit having small and very narrow high-impedance biasing lines. The RF isolation is also improved by RF choke/high-value resistor, and putting them away from the near-field of the radiating part. A combination of RF choke and DC blocking capacitor is also used which creates strong isolation between the RF and DC bypassing.

The proposed frequency reconfigurable antenna provides flexibility and adaptability for wireless communication applications. However, its implementation introduces challenges such as increased complexity, larger size, bandwidth limitations, and higher power consumption. To address these challenges, future studies may investigate alternative strategies, such as the use of advanced materials and employing active control algorithms with feedback mechanisms for switch configurations.

6. Conclusion

The suggested reconfigurable multi-band-notched antenna can operate in UWB as well as single, dual, triple, and quadruple-band notches. It might improve spectrum use and reduce interference from narrowband transmissions, including measured notch bands of 3.40-3.70 GHz (n78), 4.84-5.70 GHz (n46), 3.88-4.32 GHz (n77), 7.10-7.61 GHz (X-band downlink satellite), and 8.04-8.68 GHz (ITU-8 GHz). In the Rhombic-shaped slot, L-shaped and

Ladder-shaped stubs are placed to obtain notch characteristics in the 5G Sub-6 GHz bands n46 and n78, and for the n77, X, and ITU-8 GHz band, a C-shaped slot, an I-shaped stub, and two RSRRs are utilized. The PIN diodes embedded into the slots and stubs are used to electrically reconfigure the band-notched behavior. The suggested antenna exhibits good consistency between measured, simulated, and equivalent circuit results. It suggests that the antenna may be used for a variety of UWB applications that are resistant to interference from nearby RF systems. Furthermore, the antenna exhibits excellent omnidirectional (in xz-plane) and dipole-like (in yz-plane) radiation patterns. It offers an approximate uniform gain and radiation efficiency with an optimal value of 4.26 dBi and 86%, respectively, across 3.15-11.88 GHz, except the notch bands. According to all of these findings, the suggested antenna may be utilized in multifunctional, interference-free UWB systems.

References

[1] Federal Communications Commission. "Revision of part 15 of the commission's rules regarding ultra-wideband transmission systems", *FIRST REPORT AND ORDER FCC*, pp. 02-48, (2002).

[2] Schantz, H.G. "November. Introduction to ultra-wideband antennas", *IEEE Conference on Ultra-Wideband Systems and Technologies*, pp. 1-9, IEEE, (2003), doi: 10.1109/UWBST.2003.1267792.

[3] Stark, A., Friesicke, C., Müller, J. and et al. "A packaged ultrawideband filter with high stopband rejection", *IEEE microwave magazine*, 11(5), pp.110-117, (2010), doi: 10.1109/MMM.2010.937087.

[4] Taher, N., Zakriti, A., Amar Touhami, N. and et al. "Circular ring UWB antenna with reconfigurable notch band at WLAN/sub 6 GHz 5G mobile communication", *Microsystem Technologies*, 28(4), pp.965-972, (2022), doi: 10.1007/s00542-021-05246-9.

[5] Mewara, H.S., Deegwal, J.K. and Sharma, M.M. "A slot resonator based quintuple band-notched Y-shaped planar monopole ultra-wideband antenna", *AEU-International Journal of Electronics and Communications*, 83, pp.470-478, (2018), doi: 10.1016/j.aeue.2017.10.035.

[6] Bakariya, P.S., Dwari, S. and Sarkar, M. "Triple band notch UWB printed monopole antenna with enhanced bandwidth", *AEU-International Journal of Electronics and Communications*, 69(1), pp.26-30, (2015), doi: 10.1016/j.aeue.2014.07.023 .

[7] Shaik, L.A., Saha, C., Siddiqui, J.Y. and et al. “Ultra- wideband monopole antenna for multiband and wideband frequency notch and narrowband applications”, *IET Microwaves, Antennas & Propagation,* 10(11), pp.1204-1211, (2016), doi: 10.1049/iet-map.2016.0063.

[8] Gao, P., He, S., Wei, X. and et al. “Compact printed UWB diversity slot antenna with 5.5-GHz band-notched characteristics”, *IEEE Antennas and Wireless Propagation Letters*, 13, pp.376-379, (2014), doi: 10.1109/LAWP.2014.2305772.

[9] Ryu, K.S. and Kishk, A.A. “UWB antenna with single or dual band-notches for lower WLAN band and upper WLAN band”, *IEEE Transactions on antennas and propagation,* 57(12), pp.3942-3950, (2009), doi: 10.1109/TAP.2009.2027727.

[10] Koohestani, M., Azadi-Tinat, N. and Skrivervik, A.K. “Compact slit-loaded ACS-Fed monopole antenna for Bluetooth and UWB systems with WLAN band-stop capability”, *IEEE Access*, 11, pp.7540-7550, (2023), doi: 10.1109/ACCESS.2023.3238577.

[11] Sharma, M.M., Kumar, A., Yadav, S. and et al. “An ultra-wideband printed monopole antenna with dual band-notched characteristics using DGS and SRR”, *Procedia Technology*, 6, pp.778-783, (2012), doi.org/10.1016/j.protcy.2012.10.094.

[12] Emadian, S.R. and Ahmadi-Shokouh, J. “Very small dual band-notched rectangular slot antenna with enhanced impedance bandwidth”, *IEEE Transactions on Antennas and Propagation*, 63(10), pp.4529-4534, (2015), doi: 10.1109/TAP.2015.2456905.

[13] Wang, Z., Liu, X., Rasool, N. and et al. “Dual band- notched ultra- wideband antenna with T- shape stub”, *Electronics Letters*, 58(20), pp.747-749, (2022), doi: 10.22541/au.165511631.19397348/v1.

[14] Sarkar, D., Srivastava, K.V. and Saurav, K. “A compact microstrip-fed triple band-notched UWB monopole antenna”, *IEEE Antennas and Wireless Propagation Letters*, 13, pp.396-399, (2018), doi: 10.1109/LAWP.2014.2306812.

[15] Abbas, A., Hussain, N., Lee, J. and et al. “Triple rectangular notch UWB antenna using EBG and SRR”, *IEEE Access*, 9, pp.2508-2515, (2020), doi: 10.1109/ACCESS.2020.3047401.

[16] Sharma, M.M., Deegwal, J.K., Kumar, A. and et al. “Compact planar monopole UWB antenna with quadruple band-notched characteristics”, *Progress In Electromagnetics Research C*, 47, pp.29-36, (2014), doi:10.2528/PIERC13121909.

[17] Zhao, Z., Zhang, C., Lu, Z. and et al. “A miniaturized wearable antenna with five band-notched characteristics for medical applications”, *IEEE Antennas and Wireless Propagation Letters*, 22(6), pp.1246-1250, (2023), doi: 10.1109/LAWP.2023.3237714.

[18] Saha, C., Siddiqui, J.Y., Freundorfer, A.P. and et al. "Active reconfigurable ultra-wideband antenna with complementary frequency notched and narrowband response", *IEEE Access*, 8, pp.100802-100809, (2020), doi: 10.1109/ACCESS.2020.2997933.

[19] Nan, J., Zhao, J., Gao, M. and et al. "A compact 8-states frequency reconfigurable UWB antenna", *IEEE Access*, 9, pp.144257-144263, (2021), doi: 10.1109/ACCESS.2021.3122250.

[20] Shrimal, S., Sharma, I.B., Kalra, B. and et al. "A compact ground-slitted CPW-fed polarization reconfigurable antenna for wireless LAN applications", *2022 IEEE Microwaves, Antennas, and Propagation Conference (MAPCON)*, pp. 1393-1397, (2022), doi: 10.1109/MAPCON56011.2022.10047383.

[21] Ojaroudi, S., Ojaroudi, Y. and Ojaroudi, N. "Novel design of reconfigurable microstrip slot antenna with switchable band- notched characteristic", *Microwave and Optical Technology Letters*, 57(4), pp.849-853, (2015), https://doi.org/10.1002/mop.28980.

[22] Toktas, A. and Yerlikaya, M. "A compact reconfigurable ultra- wideband G- shaped printed antenna with band- notched characteristic", *Microwave and Optical Technology Letters*, 61(1), pp.245-250, (2019), doi.org/10.1002/mop.31516.

[23] Srivastava, G., Dwari, S. and Kanaujia, B.K. "A compact UWB antenna with reconfigurable dual notch bands", *Microwave and Optical Technology Letters*, 57(12), pp.2737-2742, (2015), doi.org/10.1002/mop.29424.

[24] Kalteh, A.A., DadashZadeh, G.R., Naser-Moghadasi, M. and et al. "Ultra-wideband circular slot antenna with reconfigurable notch band function", *IET Microwaves, Antennas & Propagation*, 6(1), pp.108-112, (2012), doi: 10.1049/iet-map.2011.0125.

[25] Magray, M.I., Muzaffar, K., Wani, Z. and et al. "Compact frequency reconfigurable triple band notched monopole antenna for ultrawideband applications", *International Journal of RF and Microwave Computer‐Aided Engineering*, 29(11), p.e21942, (2019), doi: 10.1002/mmce.21942.

[26] Nasrabadi, E. and Rezaei, P. "A novel design of reconfigurable monopole antenna with switchable triple band-rejection for UWB applications", *International Journal of Microwave and Wireless Technologies*, 8(8), pp.1223-1229, (2016), doi: 10.1017/S1759078715000744.

[27] Dalal, K., Singh, T. and Singh, P.K. "A Low Profile Ultra-Wideband Antenna Design with Reconfigurable Notch-Bands for Wideband and Narrowband Applications",

Wireless Personal Communications, 125(2), pp.1405-1423, (2022), doi: 10.1007/s11277-022-09611-3.

[28] Quddious, A., Abbasi, M.A.B., Antoniades, M.A., and et al. "Dynamically reconfigurable UWB antenna using an FET switch powered by wireless RF harvested energy", *IEEE Transactions on Antennas and Propagation*, 68(8), pp.5872-5881, (2020), doi: 10.1109/TAP.2020.2988941.

[29] Yadav, A., Kumar, G. and Yadav, R.P. "Frequency reconfigurable dual notch UWB antenna", *International Conference on Wireless Communications Signal Processing and Networking (WiSPNET)*, pp. 1-6, IEEE, (2020), doi: 10.1109/WiSPNET48689.2020.9198600.

[30] Alnaiemy, Y. and Nagy, L. "A novel UWB monopole antenna with reconfigurable band notch characteristics based on PIN diodes", *Info communications Journal*, 13(3), pp.33-44, (2021), doi: 10.36244/ICJ.2021.3.4.

[31] Sreelakshmi, K. and Rao, G.S. "A Compact Reconfigurable CPW-Fed Dual Band-Notched UWB Antenna Using PIN Diodes", *Iranian Journal of Science and Technology, Transactions of Electrical Engineering*, 47(3), pp.1153-1165, (2023), doi: 10.1007/s40998-023-00591-z.

[32] Alazemi, A.J. and Alsaleh, Y.T. "An ultrawideband antenna with two independently tunable notch bands", *Alexandria Engineering Journal*, 79, pp.402-410, (2023), doi: 10.1016/j.aej.2023.07.082.

[33] Rai, V.K. and Kumar, M. "Tunable inverted u-shaped dual band notch monopole antenna for ultrawideband applications", *IETE Journal of Research*, 69(7), pp.4451-4460, (2023), doi: /10.1080/03772063.2021.1951373.

[34] Doddipalli, S. and Kothari, A. "Compact UWB antenna with integrated triple notch bands for WBAN applications", *IEEE access*, 7, pp.183-190, (2018), doi: 10.1109/ACCESS.2018.2885248.

[35] Zhu, F., Gao, S., Ho, A.T. and et al. "Multiple band-notched UWB antenna with band-rejected elements integrated in the feed line", *IEEE Transactions on Antennas and Propagation*, 61(8), pp.3952-3960, (2013), doi: 10.1109/TAP.2013.2260119.

[36] Sharma, I.B., Joshi, P., Shrimal, S. and et al. "The Design of Multi Band Antenna with Improved Higher order mode Radiation Using CMA for L5-band, L1-band, and S-band Application", *Scientia Iranica (International Journal Science & Technology)*, (2023), doi: 10.24200/SCI.2023.62142.7669.

Figures Captions List

Figure 11. ECM model, Simulated, and Measured results (a) ECM model with no notch band (b) ECM model with quad notch bands (c) CST design studio ECM model (d) Impedance curve with no notch band (e) Impedance curve with quad notch bands (f) Simulated, measured and ECM model's reflection coefficient [S_{11}]

Table Captions List

Table 1. The specified antenna's optimized dimensions
Table 2. Parametric analysis of notch structures
Table 3. Different operating modes and notch frequency bands of the proposed antenna
Table 4. Comparison between suggested antenna with several existing designs
Table 5. Optimal RLC component value

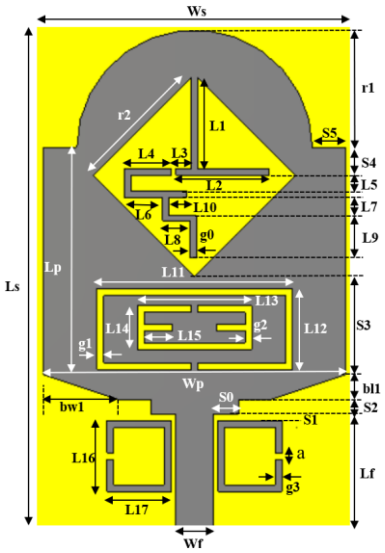

(a) Front view

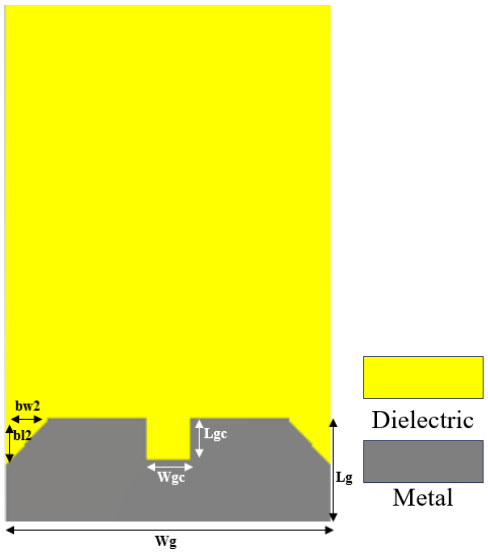

(b) Rear view

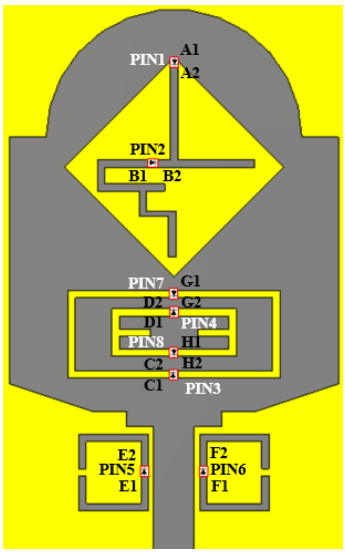

(c) Schematic diagram with reconfigurability

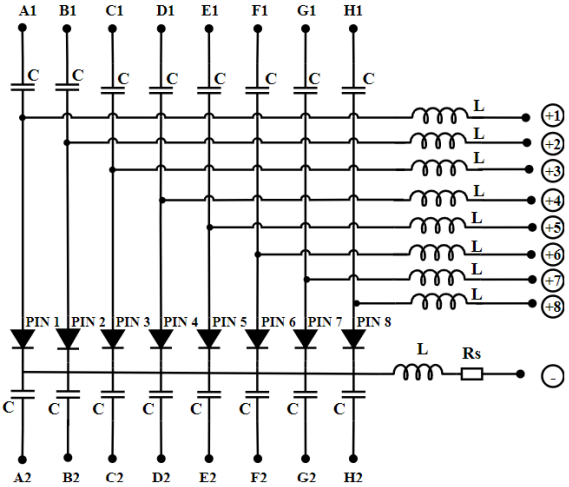

(d) Biasing circuit for PIN diodes

Figure 1. Suggested antenna's geometrical structure

(a) Antenna-1 with partial UWB bandwidth

(b) Antenna-2 with UWB bandwidth

(c) Antenna-3 with single notch band (n46)

(d) Antenna-4 with single notch band (n78)

(e) Antenna-5 with dual notch band (n78, n77)

(f) Antenna-6 with triple notch band (g) Suggested Antenna

Figure 2. Step-by-step evolution of the multi-notch band antenna

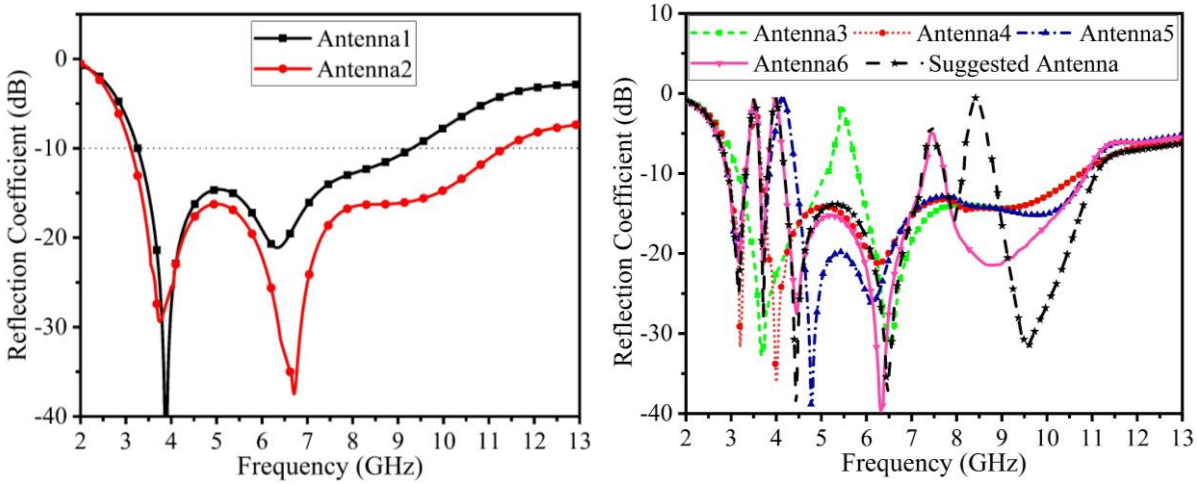

(a) Antenna-1, 2 (b) Antenna-3,4,5,6, suggested antenna

Figure 3. Reflection coefficient plot of design steps

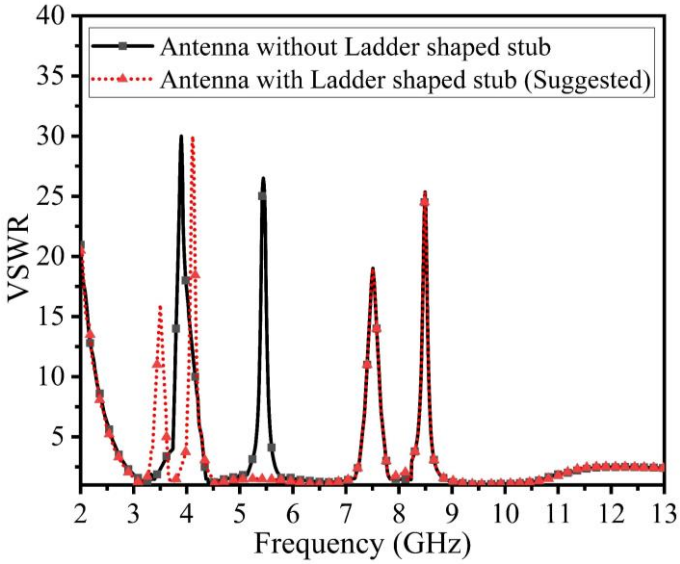

Figure 4. VSWR plot of suggested antenna

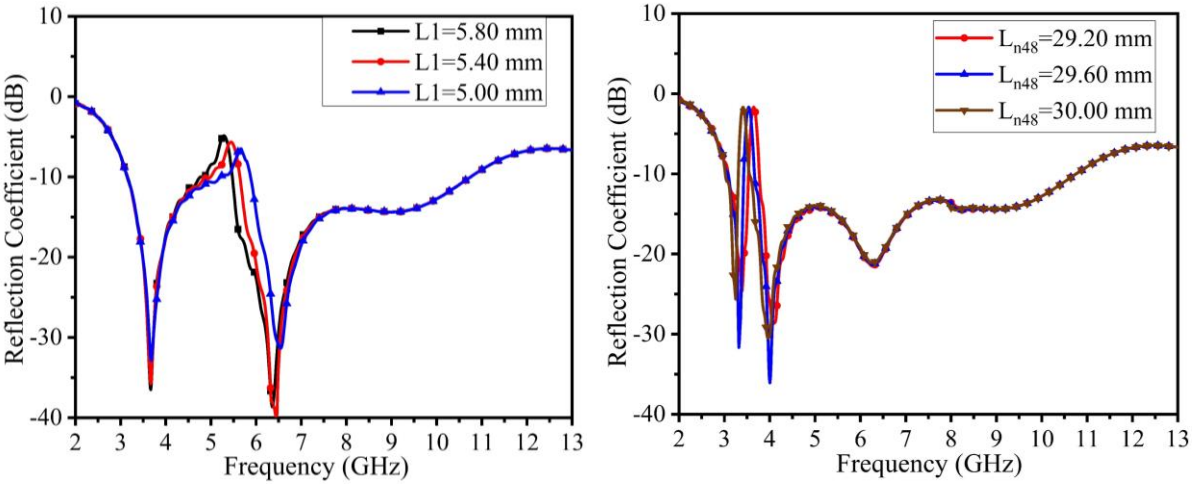

(a) (b)

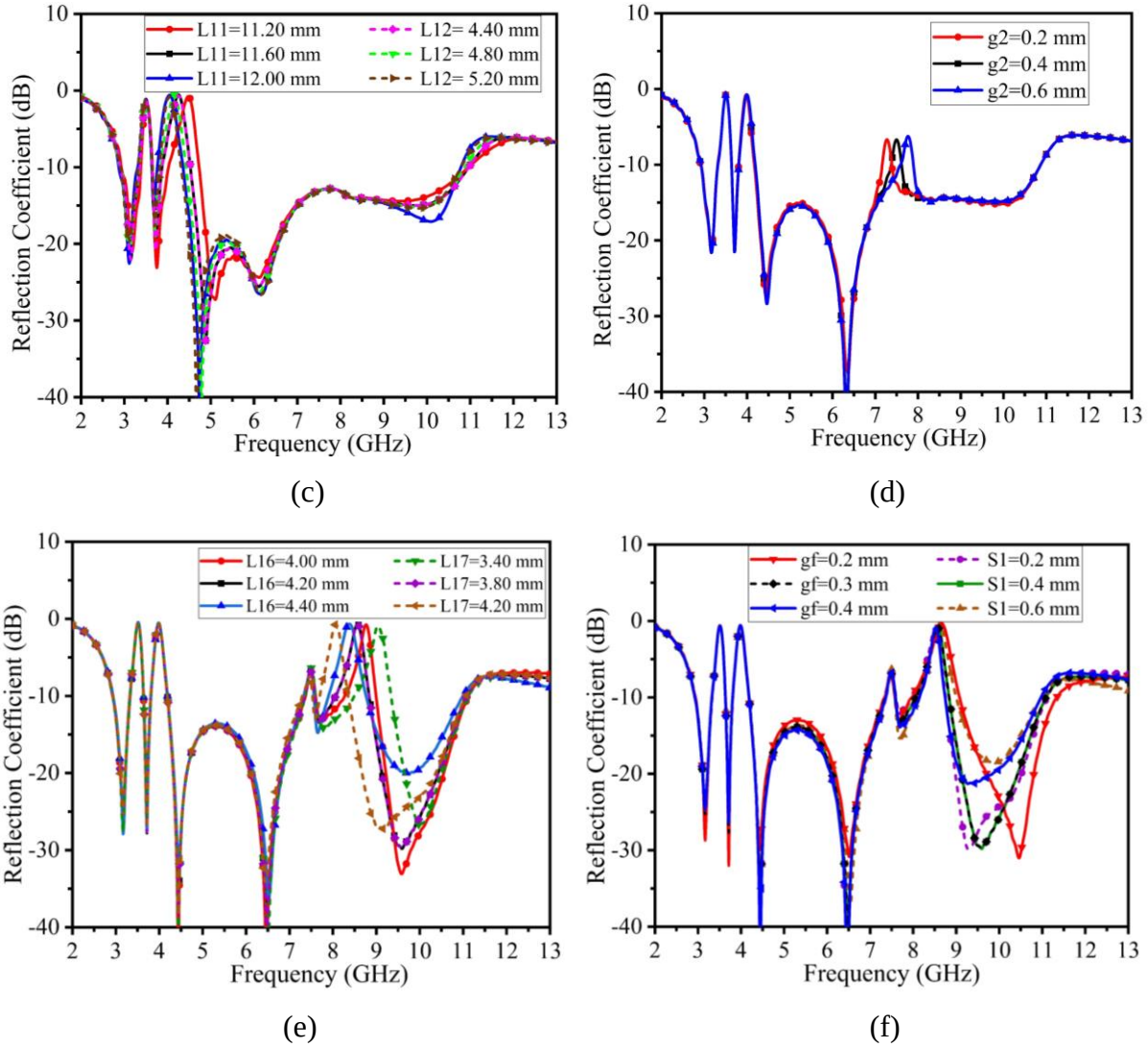

Figure 5. Parametric Variation in (a) L_1 (b) L_{n78} (c) L_1, L_2 (d) g_2 (e) L_{16}, L_{17} and (f) g_f, S_1

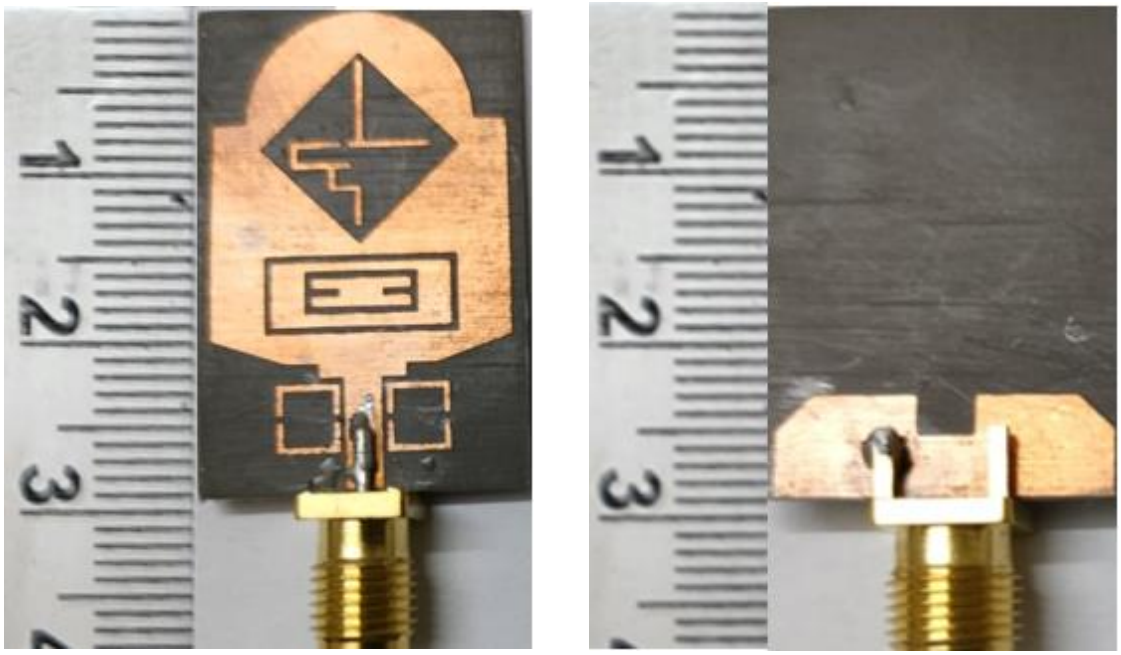

(a) (b)

(c) (d)

Figure 6. Fabricated antenna (a) Top view, (b) Rear view, (c) Circuitry for reconfiguration biasing, and (d) Antenna setup in an anechoic chamber

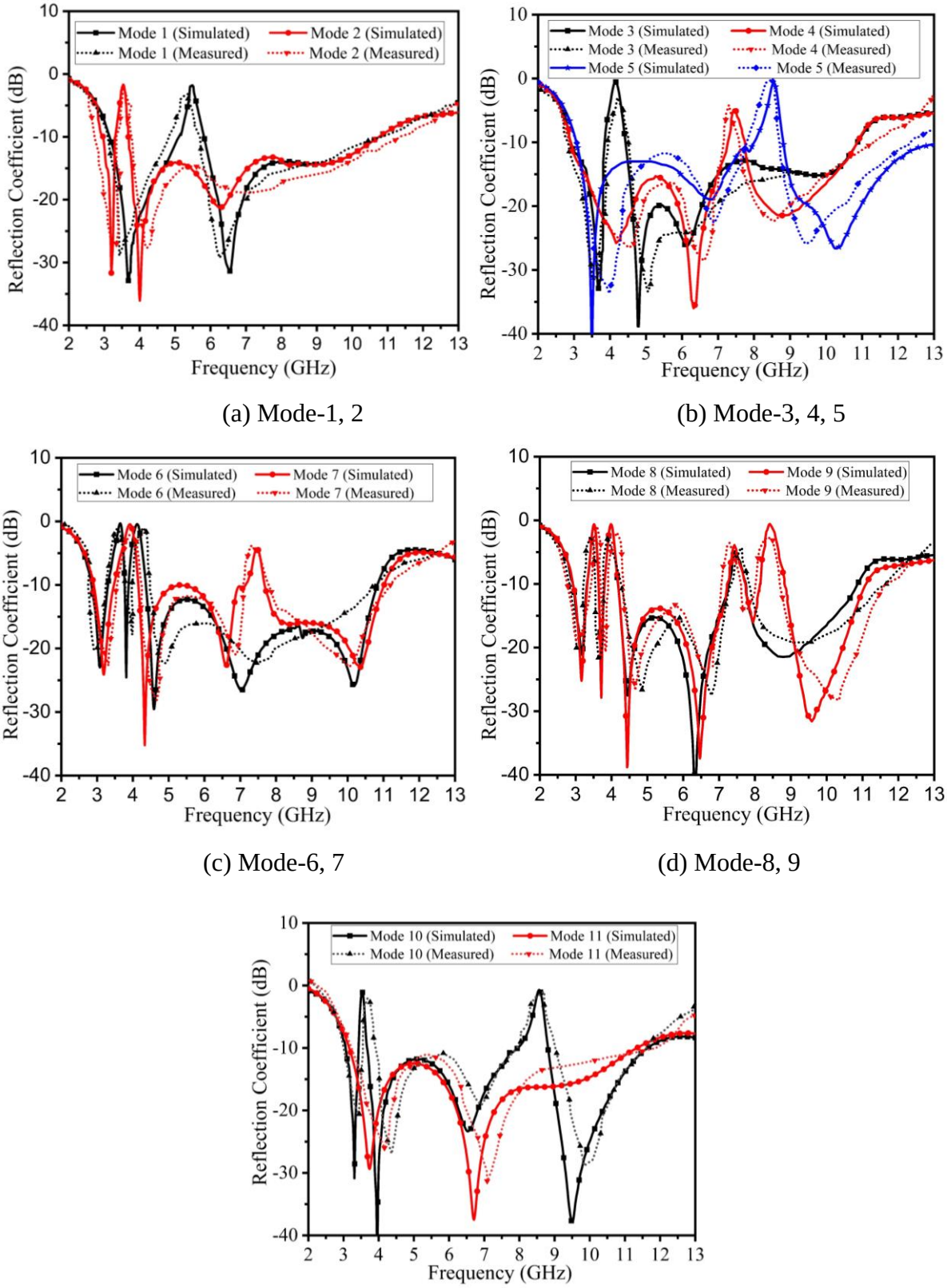

(a) Mode-1, 2

(b) Mode-3, 4, 5

(c) Mode-6, 7

(d) Mode-8, 9

(e) Mode-10,11

Figure 7. PIN diodes' switching circumstances, Reflection coefficient [S_{11}] curve with various operating modes

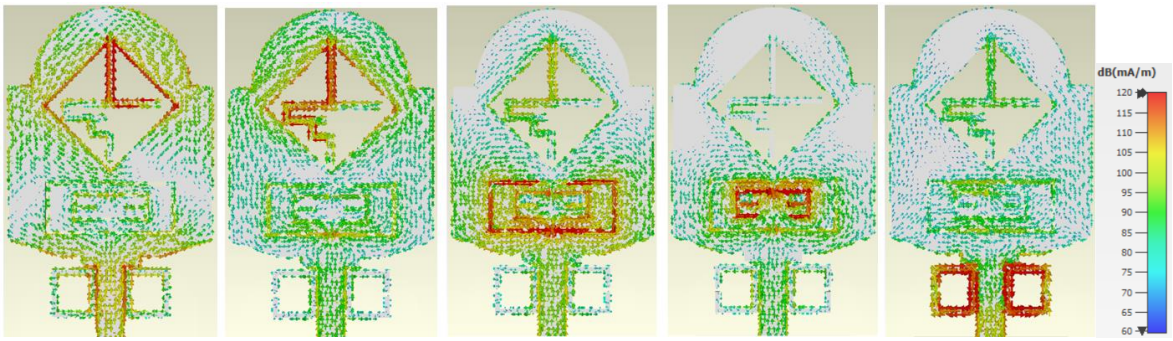

(a) 5.5 GHz (b) 3.5 GHz (c) 4.1 GHz (d) 7.5 GHz (e) 8.5 GHz

Figure 8. Surface current at different notched frequencies

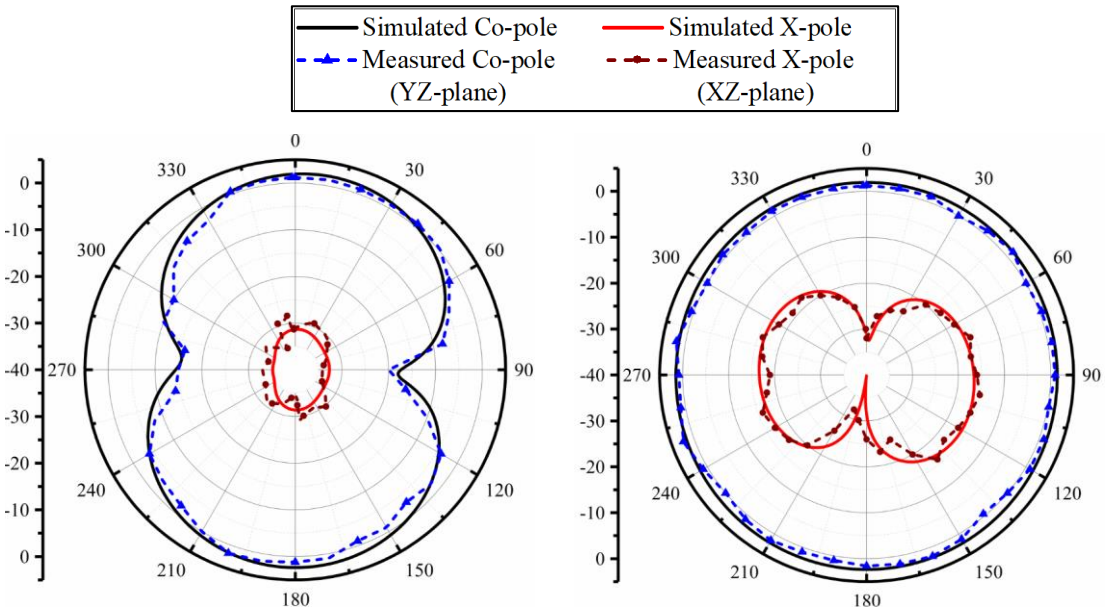

(a) 3.7 GHz

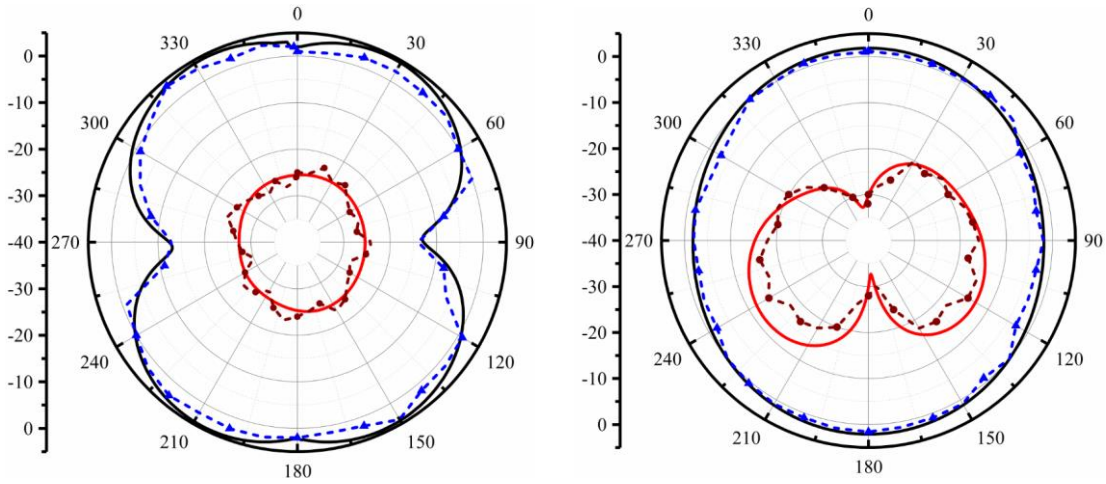

(b) 6.4 GHz

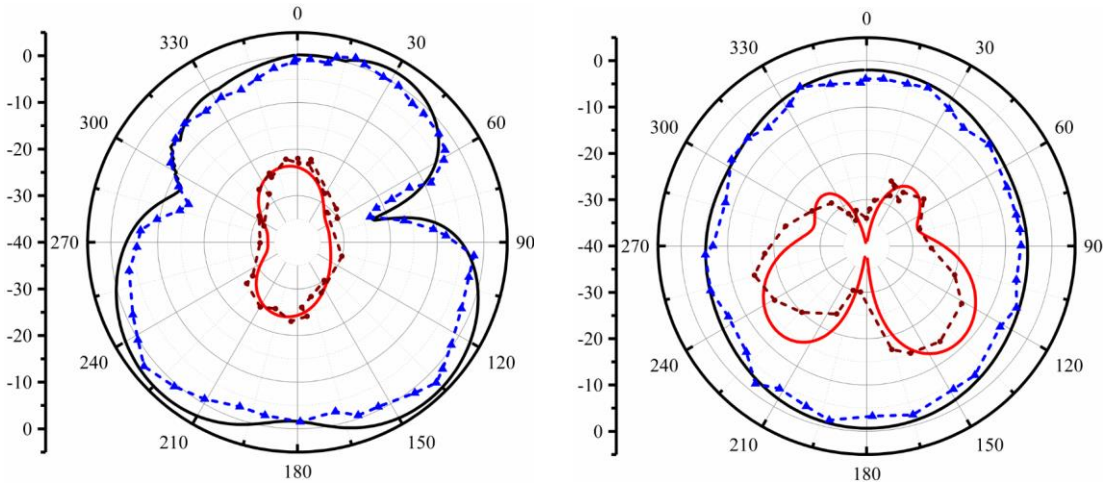

(c) 9.5 GHz

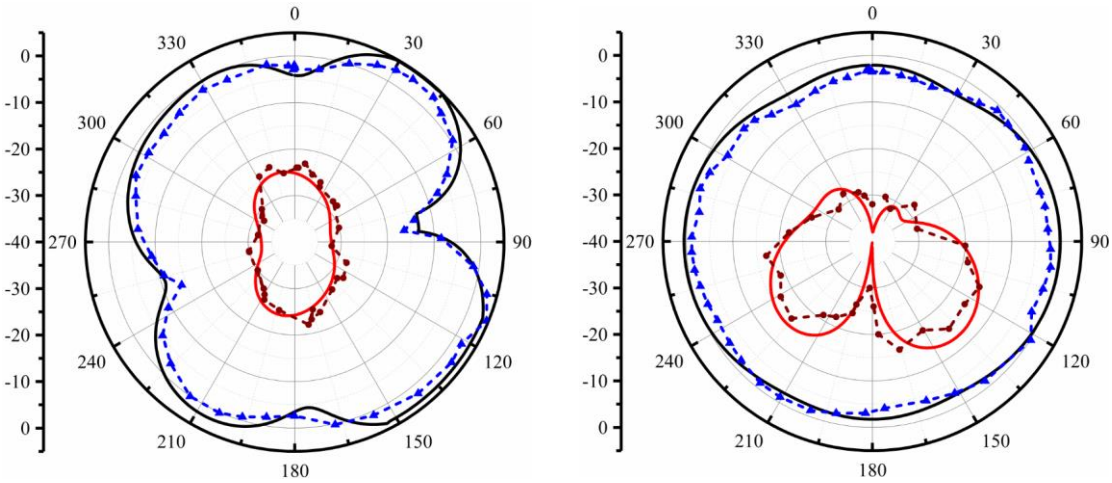

(d) 11 GHz

Figure 9. Simulated and measured radiation patterns at different pass-band frequencies.

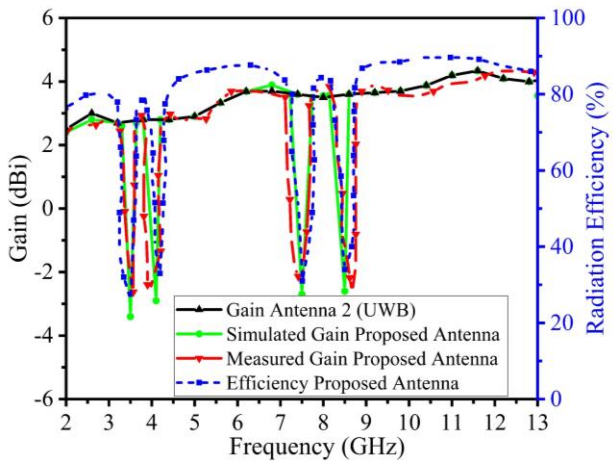

(a) Gain and radiation efficiency

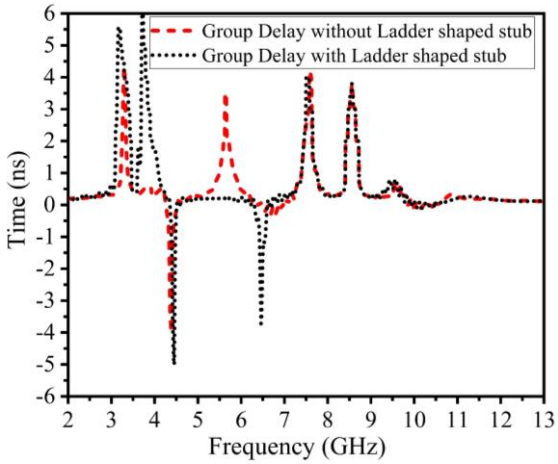

(b) Group delay

Figure 10. Simulated and measured results

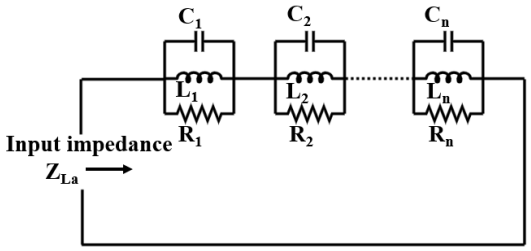

(a) ECM model with no notch band

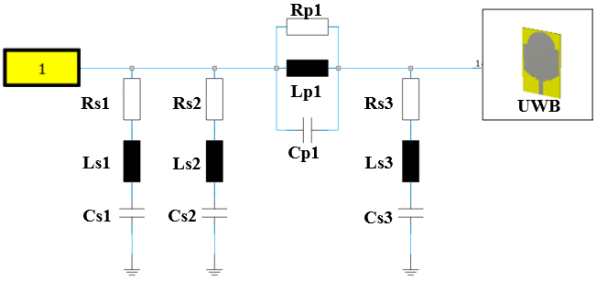

(b) ECM model with quad notch bands

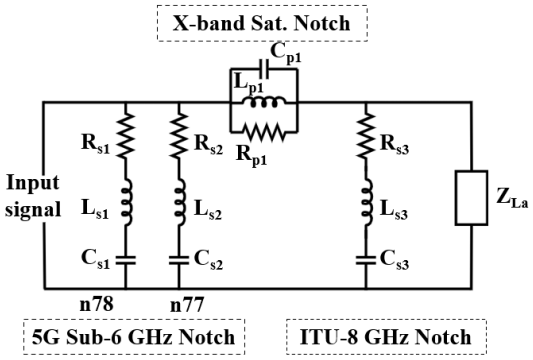

(c) CST design studio ECM model

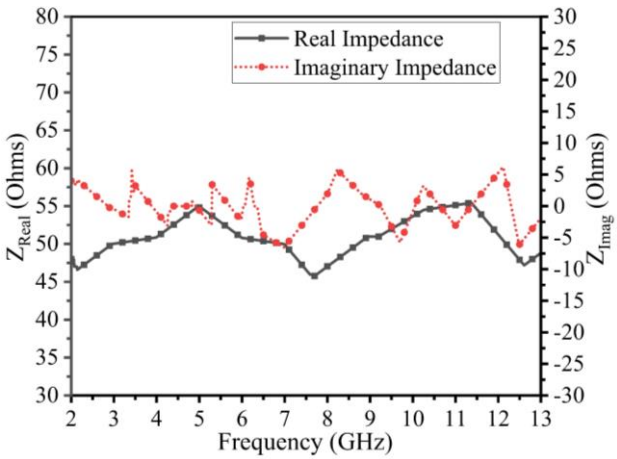

(d) Impedance curve with no notch band

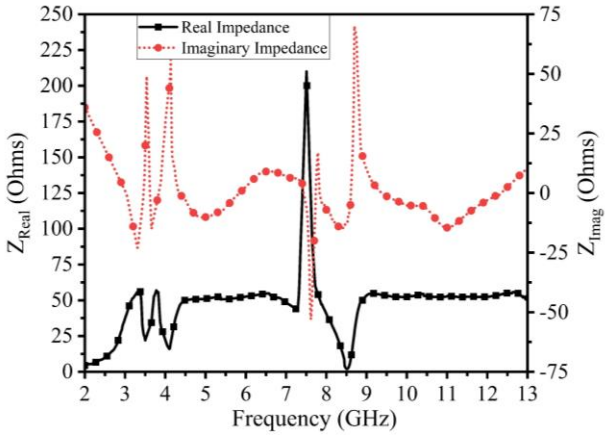

(e) Impedance curve with quad notch bands

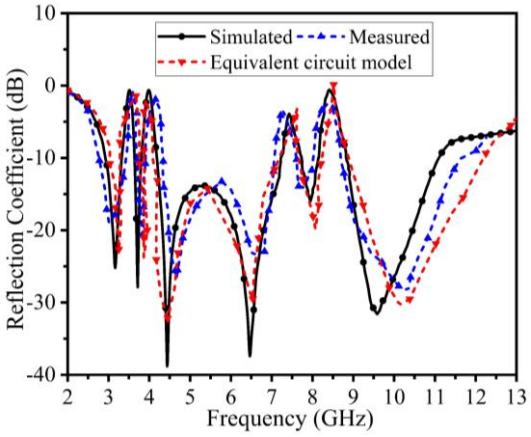

(f) Simulated, measured and ECM model's reflection coefficient [S_{11}]

Figure 11. ECM model, Simulated, and Measured results

Table 1. The specified antenna's optimized dimensions

Parameters	W_s	L_s	W_p	L_p	W_f	L_f	S_0	S_1	S_2	bw_1	bl_1	L_1	L_2	L_3
Unit (mm)	18.5	29.5	18	13.	2.2	6.8	1.49	0.4	0.85	4.2	1.8	5.2	7.6	0.5
Parameters	L_4	L_5	L_6	g_0	g_1	g_2	L_7	L_8	L_9	r_1	r_2	W_g	L_{10}	L_{11}
Unit (mm)	8.1	1.7	2.3	0.4	0.4	0.4	1.4	1.6	2.2	7	8.49	18.	2	10.6
Parameters	L_{12}	L_{13}	L_g	W_g	L_{gc}	bw_2	bl_2	S_3	S_4	S_5	L_{14}	L_{15}	L_{16}	L_{17}
Unit (mm)	4.8	6.8	6	2.6	2.91	1.8	2.2	5.8	1.6	2	2.6	1.7	4.2	3.8

Table 2. Parametric analysis of notch structures

SN	Band Notch Structure (BW)	Parameter variation	Bandwidth variation	Optimized Value (mm)	VSWR at f_{Notch}
1.	L-shaped stub (5.15-5.82 GHz)	L_1 (4.6 to 5.8 mm), 0.4 step size at L2 = 4.7 mm	(5.63–6.07 GHz) to (4.86–5.41 GHz)	L_1 = 5.4	27.30 at 5.5 GHz
		L_2 (4.3 to 5.5 mm), 0.4 step size at L1 = 5.4 mm	(5.82 – 6.30 GHz) to (5.10–5.64 GHz)	L_2 = 4.7	
2.	L- shape-Ladder-shaped stub (3.30-3.68 GHz)	L_{n78} (28.8 to 30.0 mm), 0.4 step size at g0=0.4 mm	(3.51-3.89 GHz) to (3.10 – 3.47 GHz)	L_{n78}=29.6	16.30 at 3.5 GHz
3.	C-shaped slot (3.80-4.40 GHz)	L_{11} (11.2 to 12.0 mm), 0.4 step size at L12 = 4.8 mm	(4.0–4.73 GHz) to (3.76-4.36 GHz)	L_{11} = 11.6	31.80 at 4.1 GHz
		L_{12} (4.4 to 5.2 mm), 0.4 step size at L_{11}=11.6 mm	(3.87–4.53 GHz) to (3.82-4.32 GHz)	L_{12} = 4.8	
		g_1 (0.3 to 0.5 mm), 0.1 step size	(3.82-4.37 GHz) to (3.89-4.58 GHz)	g_1 = 0.4	
4.	I-shaped stub (7.25-7.75 GHz)	L_{13} (6.4 to 7.2 mm), 0.4 step size at L_{14}= 2.6 mm	(7.92-8.27 GHz) to (6.88-7.15 GHz)	L_{13} =6.8	17.80 at 7.5 GHz
		L_{14} (2.4 to 2.8 mm), 0.2 step size at L_{13} =6.8 mm	(7.60-7.90 GHz) to (7.09-7.33 GHz)	L_{14}= 2.6	
		g_2 (0.3 to 0.6 mm), 0.1 step size.	(7.15-7.38 GHz) to (7.81-8.22 GHz)	g_2=0.4	
5.	RSRRs (8.14-8.83 GHz)	L_{ITU} (14.4 to 16.8 mm), 0.4 step size	(8.36-9.05 GHz) to (7.92-8.61 GHz)	L_{ITU} =15.6	25.20 at 8.5GHz
		g_f (0.2 to 0.5 mm), step size 0.1 mm at L_{ITU} = 15.6 mm	(8.0-9.9 GHz) to (8.15-8.74 GHz)	g_f = 0.4	
		S_1 (0.2 to 0.6 mm), 0.2 step size	(8.0-8.75 GHz) to (8.12-9.33 GHz)	S_1 = 0.4	

Table 3. Different operating modes and notch frequency bands of the proposed antenna

Operating Mode	Switch Configuration								Notch Bands	Notch band (GHz)	
	D 8	D 7	D 6	D 5	D 4	D 3	D 2	D 1		Simulated	Measured
Mode -1	on	on	off	off	on	on	off	on	Single	$(5.15–5.82)^0$	$(4.84\text{-}5.70)^0$
Mode -2	on	on	off	off	on	on	on	on	Single	$(3.30–3.68)^1$	$(3.34–3.75)^1$
Mode -3	off	off	off	off	off	on	off	off	Single	$(3.80–4.40)^2$	$(3.93–4.51)^2$
Mode -4	off	off	off	off	on	off	off	off	Single	$(7.25–7.75)^3$	$(7.14–7.59)^3$
Mode -5	on	on	on	on	on	on	off	off	Single	$(8.14–8.83)^4$	$(7.85–8.70)^4$
Mode -6	off	off	off	off	off	on	on	on	Dual	$(3.30–3.68)^1$ $(3.80–4.40)^2$	$(3.24–3.78)^1$ $(3.97–4.47)^2$
Mode -7	off	off	off	off	on	on	off	off	Dual	$(3.30–4.20)^1$ $(7.25–7.75)^3$	$(3.55–4.26)^1$ $(7.10–7.80)^3$
Mode -8	off	off	off	off	on	on	on	on	Triple	$(3.30–3.68)^1$ $(3.80–4.20)^2$ $(7.25–7.75)^3$	$(3.22–3.55)^1$ $(3.75–4.28)^2$ $(7.30–7.86)^3$
Mode -9	off	off	on	on	on	on	on	on	Quad	$(3.30–3.68)^1$ $(3.80–4.20)^2$ $(7.25–7.75)^3$ $(8.14–8.83)^4$	$(3.40–3.70)^1$ $(3.88–4.32)^2$ $(7.10–7.61)^3$ $(8.04–8.68)^4$
Mode -10	on	on	on	on	on	on	on	on	Dual	$(3.42\text{-}3.67)^1$ $(8.00\text{-}8.82)^4$	$(3.55\text{-}3.90)^1$ $(7.93\text{-}8.95)^4$
Mode 11	on	on	off	off	on	on	off	off	No Notch	(3.10-11.67) (Full UBW)	(3.15-11.88) (Full UBW)
Note: 0- n46 band, 1 – n78 band, 2 -n77, 3 –X-band, and 4 –ITU-8 GHz band											

Table 4. Comparison between suggested antenna with several existing designs

Ref. No. (Year)	Size (mm^3)	Substrate, ϵ_r	Impedance BW (GHz)	Switch Type	No. of switches	No. of notches	Notched Bands (Frequency range)	Peak Gain (dBi)
[4] (2022)	10 x 28 x 1.6	FR4, 4.3	3.1-12.3	PIN diode	3	3	5G-Sub 6(3.4-3.8 GHz) 5G-Sub 6(3.8-4.9 GHz) WLAN (5.10-5.80 GHz)	-
[27] (2022)	24 x 24 x 1.6	FR4, 4.4	3.1-10.6	Metal strip	5	4	Wi-MAX (3.31-3.65GHz) C-band (4.90-5.56 GHz) WLAN (5.90-6.40 GHz) X-band (7.30-8.50 GHz)	5.0
[28] (2020)	33 x 27 x 0.787	RT/ Duroid 5880, 2.2	2.4-12	FET	1	1	WLAN (5.0-6.0 GHz)	4.3
[29] (2020)	36 x 46 x 1.6	FR4, 4.4	3.0-11	PIN diode	4	2	Wi-MAX (3.80-4.20) WLAN (5.10-5.80)	2.0
[30] (2021)	50 x 60 x 1.6	FR4, 4.3	1.86-10.89	PIN diode	3	3	Wi-Fi (2.74-3.94 GHz) WLAN (5.44-6.38 GHz) X-band (7.54-8.40 GHz)	5.2
[31] (2023)	24 x 20 x 0.787	FR4, 4.4	2.7-11.4	PIN diode	2	2	S-band (2.85–3.34 GHz) WLAN (4.9–5.64 GHz)	3.2
[32] (2023)	21.5 x 48 x 1.524	RO4003 C, 3.55	3.1-11.0	Varactor	4	2	WLAN (5.08 -5.77 GHz) X-band (7.75-8.52)	3.7
[33] (2023)	36 x 30 x 0.762	RT/duroid 5880, 2.2	2.6-14.0	Varactor	3	2	WLAN (5.58-5.91 GHz) C-band (7.02-7.45 GHz)	2.89
This work	18.5 x 29.5 x 0.762	RT/duroid 5880, 2.2	3.1-11.67	PIN diode	8	5	5G-n78 (3.30–3.68 GHz) / 5G-n46 (5.15–5.82 GHz) 5G-n77 (3.80 – 4.40 GHz) X-band (7.25–7.75 GHz) ITU-8 GHz (8.14–8.83 GHz)	4.26

Table 5. Optimal RLC component value

Components	Value(Ω)	Components	Value(nH)	Components	Value(pf)
R_{s1}	22	L_{s1}	10	C_{s1}	0.20
R_{s2}	16	L_{s2}	5	C_{s2}	0.30
R_{p3}	210	L_{p3}	0.25	C_{p3}	1.80
R_{s4}	6	L_{s4}	1.50	C_{s4}	0.23

Subhash Shrimal received a B.E. degree in Electronics and communication engineering from the University of Rajasthan, Jaipur, India, in 2005 and an M.Tech. degree in Electronics and communication engineering from Malviya National Institute of Technology, Jaipur, India, in 2008. He is currently working toward his PhD degree at MNIT Jaipur since 2020. He is presently working as a Lecturer at Government Polytechnic College, Board of Technical Education Rajasthan. His main areas of interest are microstrip and reconfigurable planar antennas.

Renu Agrawal is a Lecturer in the Department of Electrical Engineering of Shri. Goku Verma Polytechnic College Bharatpur Rajasthan, India. She received her B.E. Degree in ECE from Mody College of Engineering & Technology Lakmangadh Sikar, Rajasthan, India, in 2003, and her M.Tech. Degree in VLSI Design from MNIT, Jaipur, Rajasthan, India in 2009. She is pursuing a Ph.D. in the area of Micro-strip Patch Antenna Design from Malaviya National Institute of Technology (MNIT), Jaipur, Rajasthan, India.

Indra Bhooshan Sharma received B.Tech. in 2013 from JNIT, Jaipur, India. He did M.Tech. in 2016 from GECA, Ajmer, India, and presently, he is PhD scholar from MNIT, Jaipur, India. He joined as Guest Faculty in the Department of ECE, MNIT, Jaipur, in 2016 and was designated as a PA-III in the CSIR-CEERI, Pilani, in 2018. He is an active Member of IEEE, including Antenna and Propagation Society. He is the author/coauthor of more than 40 research papers published in refereed international/ national journals and conferences. His research interests include planar UWB antennas, circularly polarized antennas, Reconfigurable antennas, and so forth.

Joohi Garg (Member IEEE) received B.Tech in Electronics and Communication Engineering from ACEIT, Jaipur, India (2011) and M.Tech in 2013 from Mody Institute of Technology and Science, Rajasthan, India. She received a Ph.D. degree from Malaviya National Institute of Technology, Jaipur, in 2023. Her research interests include FSS, Metamaterials, Absorbers, Resorbers, Conformal Antenna etc.

Mahendra Mohan Sharma received a B.E. degree in 1985 from NIT, Srinagar, India. He did an M.Tech. from IIT, Delhi, and PhD from MNIT, Jaipur, India. He joined as a Lecturer in the Department of Electrical Engineering, MNIT, Jaipur, in 1986 and was designated as an Associate Professor there in 1995. Presently, He is working as a Professor with the Department of Electronics and Communication Engineering, MNIT Jaipur. Besides being an able academician and administrator (Registrar in MNIT and Ex Executive Director at National Institute of Electronics and Information Technology, Chandigarh). He is an active member of IEEE, Broadcasting Engineering Society (India), and a Life Senior Member of ISTE professional bodies. He is the Honorary Secretary of the IEEE-MTTS India Council Chapter. He is the author/coauthor of more than 100 research papers published in international/national journals and conferences. His research interests include the design and modeling of antennas, arrays, and FSS.